Effect of Yb-substitution on thermally activated flux creep in the $Bi_2Sr_2CaCu_{2-x}Yb_xO_y$ superconductors

H. Gundogmus[1], B. Ozcelik[1], A. Sotelo[2], M. A. Madre[2]

[1]Department of Physics, Faculty of Sciences and Letters, Cukurova University, 01330 Adana, Turkey

[2]ICMA, CSIC-Universidad de Zaragoza, Marı´a de Luna, 3, 50018 Zaragoza, Spain

Abstract In the present work, $Bi_2Sr_2CaCu_{2-x}Yb_xO_y$ (x = 0.0, 0.05, 0.1, and 0.25) superconductors were prepared by a polymer matrix route technique, and subsequently used as feed in a laser induced directional solidification (LFZ) process. The X-ray diffraction, DC magnetization and magnetoresistance measurements were studied. All samples consist mainly of the Bi-2212 phase which indicates the performed process is adequate. However, some impurity phases like $CaCuO_2$ were also detected. We have calculated the hole number using the relation given by Presland, and particle size, Lhkl, using the XRD patterns results. From M–T results, the superconducting transition temperatures, T_C, of the samples were found 93, 90, 87, and 85 K, respectively. The activation energies, irreversibility fields (H_{irr}), upper critical fields (H_{c2}) and coherence lengths at 0 K ($\xi(0)$) were calculated from the resistivity versus temperature (R–T) curves, under DC magnetic fields up to 5 T. The thermally activated flux creep model has been studied in order to calculate the flux pinning energies. The results indicated that $H_{c2}(0)$ varied from 132 to 30 T and the flux pinning energies varied from 650 to 400 meV at 0 T, with the content of Yb.

Corresponding author: H. Gundogmus. Department of Physics, Faculty of Sciences and Letters, Cukurova University, 01330 Adana, Turkey. e-mail: hkngundogmus@gmail.com

1 Introduction

Since the discovery of high-temperature superconductors, many substitutions have been made in BSCCO system in order to improve their physical and magnetic properties [1–17]. The effect of substitution on the Cu sites is more important than other ones since the transition temperature in ceramic superconductors depends on the charge carrier concentration in the Cu–O planes. It is well-known that holes in the Cu–O planes created by electron doping constitute an important parameter to achieve superconductivity. There are three phases in the Bi-based superconductors with general formula $Bi_2Sr_2Ca_{n-1}Cu_nO_y$ where n = 1, 2, and 3. The transition temperatures of these different phases are related to the numbers of the Cu–O layers per unit cell [18].

It is rather difficult to realize the mixed state of high temperature superconductors due to their short coherence length, large anisotropy and thermal energy. After the first prediction of flux creep by Anderson [19], large amounts of the research have been recently addressed to the effect of applied external magnetic field on resistive transition in order to better understand the mechanism of flux pinning and flux motion [20–26]. There are several models for understanding of resistivity broadening under a magnetic field, such as thermally activated flux creep [22], flux flow [21], flux line melting and flux cutting [27], etc. The flux line can be thermally activated over the pinning energy barrier, even if the Lorentz force exerted on the flux bundle by the current is smaller than the pinning force. Some researchers have pointed out that a thermally activated flux creep model can describe the data quite well for resistivity region near T_C ($\rho = 0$) [24, 28–31].

In addition, the material preparation technique plays a crucial role [32], as important as the substitutions creating a pinning center in BSCCO systems. Moreover, these HT_C systems possess a high crystallographic anisotropy which can be exploited by an adequate grain alignment to produce high quality tapes and wires, as well as bulk materials with improved electrical properties. In order to obtain very quick and homogeneous sample, one of best methods is the polymer matrix route [33–35]. Other techniques used to improve the transport properties are based on the grain orientation [36, 37]. Among all these techniques, the Laser

Floating Zone Melting (LFZ) technique has been shown as a very reliable process to obtain well-aligned Bi-2212 grains, with their c-axis nearly perpendicular to the growth direction, and very small amounts of secondary phases [38–43].
In previous studies the mechanical, physical and superconducting properties of Yb-substituted LFZ prepared samples [18] indicated that Yb substitution is responsible for the variation in both magnetic and superconducting properties. In this work, the magnetoresistance of Yb-substituted samples is studied. Moreover, the thermally activated flux creep model has been applied on the resistivity curves under various applied magnetic fields between 0 and 5 T.

2 Experimental details

The preparation technique has been explained in detail in previous works [18]. Phase determination was performed on annealed samples using X-ray powder diffraction measurements (Rigaku D/max-B). Electrical measurements were performed by the conventional four-point probe configuration on about 30 mm long samples. Magnetoresistivity measurements were carried out under various applied magnetic fields of 0, 0.5, 1, and 5 T. Upper critical magnetic field (H_{c2}) values of the samples were calculated from the R-T curves. The temperature dependence of the magnetization (FC and ZFC) has been measured under 50 Oe external field, by using a 7304 model Lake Shore VSM system. The samples with x = 0.0, 0.05, 0.1, and 0.25 will be hereafter named as A, B, C, and D, respectively.

3 Results and discussion

The normalized XRD diffraction patterns of samples are shown in Fig. 1. In these plots, it can be seen that the major peaks (indicated in Fig. 1 by ?) correspond to the Bi-2212 phase independently of the amount of the Yb doping [44]. Moreover, small amounts of $CaCuO_2$ nonsuperconducting secondary phase (indicated in Fig. 1 by *) have also been detected in the samples. From these data, it is observed that the crystal symmetry of all the samples is tetragonal and the obtained lattice parameters are calculated using the least squares method and presented in Table 1. As it can be inferred from these data, while a-b parameters which can be

associated to the in-plane Cu–O bond length, are unchanged, c-parameter is decreased with increasing Yb concentration. It is argued that the variation of the oxygen content on the lattice structure by substituting Yb for Cu ions can cause the reduction in the c-parameter. In addition, no Yb-contained phase is was observed, indicating that Yb atoms are incorporated into the crystal structure of Bi-2212 superconductor [45–47]. On the other hand, the XRD patterns are very similar for all the samples prepared with only minor differences in the relative intensity for some diffraction peaks were observed due to the plate-like surface structure of the sample.

The temperature dependence of both FC and ZFC magnetizations of the samples has been measured and given in Fig. 2, under an external applied magnetic field of 50 Oe. It can be deduced that the field cooled (FC) samples show a decrease on the superconducting properties. According to ZFC data, the samples become diamagnetic below their onset temperatures of 93, 90, 87 and 85 K, respectively, and diamagnetic saturation is almost reached at the lowest temperatures. These behaviors are mainly caused by their granular nature, together with the effect of the secondary phases, thus the grain boundaries show weak connectivity [48].

In order to get more information about the crystal sizes, the Debye Scherer formula [49] has been applied to the XRD data, discussed previously, which is given by:

$$\mathrm{L_{hkl}} = 0.9\lambda/\beta\cos\theta$$

where k is the used wavelength, b is the full width at half maximum and h is the angle of the peak. As can be seen from Table 1, the particle sizes decrease with increasing Yb content. The number of holes, p, per Cu atom can be calculated by using the relation

$$\frac{T_c}{T_c^{\max}} = 1 - 82.6(p - 0.16)^2$$

given by Presland et al. [50], where T_c^{max} is taken as 85 K for the Bi-2212 system and T_c^{offset} values are obtained from the zero field resistivity measurements given in Table 2. The results show that the p values of the samples are ranging from 0.144 to 0.135 (see Table 1). It is clear that the hole-concentration decreases with

increasing Yb substitution. This is due to the fact that Yb substitution reduces the number of holes per Cu atom and diminishes the superconducting properties of the system. This is in agreement with our previously reported results [44].

Variation of resistivity as a function of temperature, under externally applied magnetic fields between 0 and 5 T, has been measured. The external DC magnetic fields for resistivity measurements were provided by an electromagnet and they were applied parallel to the current direction. Zero field cooling (ZFC) procedure was used during all measurements. The results obtained are presented in Fig. 3 for various applied magnetic fields. The samples exhibit a metallic-like behavior above the critical temperature. In addition, the onset (T_c^{onset}) and offset (T_c^{offset}) critical temperature values were evaluated by using the magnetoresistance curves given in Fig. 3. As it is well known T_c^{onset} temperature is related to the transition of isolated grains to the superconducting state. On the other hand, T_c^{offset} temperature is related to volume fraction of Bi-2223 phase and/or features of intergranular component [24, 51–53]. Therefore, the temperatures close to the onset transition temperature region, the structure is in accordance with the intergrain transitions, and these transitions are not affected by the applied magnetic field due to the absence of flux traps. As a result, since the flux or vortex pinning is ineffective in this region, and substantial variation in the T_c^{onset} temperature value is not expected in the presence of the magnetic field [28, 54, 55]. On the other hand, in the vicinity of the offset temperature T_c^{offset}, the resistivity of the sample depends upon the applied magnetic field as a consequence of the thermally activated flux flow (TAFF) process. Therefore the pinning of vortices will be highly effective in this region.

T_c^{onset} and T_c^{offset} values obtained at different applied magnetic field strength were given in Table 2. As can be seen from the table, T_c^{onset} values of the samples dramatically decrease from 100 to 97 K for sample A, from 98.6 to 92 K for sample B, from 97.7 to 86 K for sample C and from 96 to 82 K for sample D. We have observed the broadening effect at the tail part of the resistivity curves and T_c^{offset} temperatures shift toward the lower temperatures by increasing the applied

magnetic field up to 5 T. T_c^{offset} values range from 95 to 78 K for A sample, from 93.2 to 63 K for B sample, from 92.1 to 56 K for C sample and from 90 to 48 K for D sample. The considerable reduction of the critical transition temperatures may be related to not only the decrement in pinning ability but also increment in the weak links between the superconducting grains and motion of fluxons [56]. In high-T_c superconductors, the efficient pinning centers are formed by defects such as dislocations, twin planes, grain boundaries, additionally to by artificial, radiation-induced columnar defects [57–60]. The nature of pinning centers mainly depends on the grain boundaries, impurities and oxygen vacancies in Cu–O layers. On the other hand, when the driving Lorentz force per unit volume, F_L = I x B exceeds the pinning force per unit volume F_P, in type-II superconductors, electric field arises, electrical resistance and hence energy dissipation occurs. At lower temperature, a higher magnetic field is required to depin the flux line since lowering the temperature increases the pinning force [57]. As a result, a shift of the zero resistivity temperature occurs [24].

In Fig. 4, the irreversibility magnetic field values, deduced from the resistivity measurements, are displayed versus the onset and offset temperatures for the samples A, B, C, and D. It is easily observed that the irreversibility field values shift towards lower temperatures with increasing Yb-content. Additionally, comparing the position of the irreversibility field lines, it is seen that the position of sample A is higher than that of others, implying that pinning ability of sample A is stronger than that of others. These results are in agreement with previous study [24]. It is generally proposed that the superconductivity is destroyed when the amount of the rare earth ions are increased in Bi-2212 superconducting system. The intergrowth of the impurity solid solution phases and formation of weak coupling between the impurity and superconducting grains plays a crucial role in diminishing the superconductivity. On the other hand, the optimum applied magnetic field may hinder the negative effect arising from the impurities. If the resistivity results are examined, one can see that the T_c^{offset} values start rising towards the higher temperature values. So it may be concluded that the effects of the impurities are shielded by the magnetic field [61].

The upper critical fields of samples are found by using the $\rho = \rho_N$ (90 %) relation, where ρ_N is the normal state resistivity at the critical temperature, T_c^{onset}, related to each field value [62]. Taking the onset temperature points of Fig. 3 as the upper critical field, $H_{C2}(T)$ values are plotted in Fig. 5. $H_{C2}(0)$ is the upper critical magnetic field at the temperature T = 0 K and can be estimated by using Werthomer-Helfond-Hohenberg (WHH) Formula [63] given as:

$$H_{C2}(0) = -0.693 Tc \left(\frac{dH_{c2}(T)}{dT} \right)_{Tc}$$

Taking T_c values found at zero field in Table 2, one can roughly calculate $H_{C2}(0)$ values as 132, 62, 56 and 30 Tesla (see Fig. 6) for the samples A, B, C, and D, respectively. It is easily seen that the $H_{C2}(0)$ values decrease from 132 to 30 Tesla, with the increasing amount of Yb-content. In our previous study, it was reported that increasing of Yb, decreasing of the critical current density and the critical temperatures [18]. These results are now more understandable with the decreasing of $H_{C2}(0)$ values. Now it is possible to calculate the coherence length, n, which is one of the characteristic parameter of the superconductors. It is an arduous quantity to measure directly, but it is thus often calculated from the equation,

$$H_{c2}(0) = \Phi_0 / 2\pi\xi^2$$

where Φ_0 is the quanta of flux ($2.07.10^{-15}$ Tm^2) [64]. Figure 6 also shows the coherence lengths values of the samples in the temperature T = 0 K calculated from equation given above. $\xi(0)$ varied from 33 to 16 Å with the content of Yb. Similar results are reported for the coherence length $\xi(0)$ and H_{C2} (0) values for Bi-based superconductors [19,25,65,66].

According to the thermally activated flux creep model, the energy dissipated in the tail part of the magnetoresistance plot is expressed by an Arrhenius-type equation [25,67–70].

$$\rho[\mathrm{H,T}] = \rho_0 \exp[-U(H)/k_B T]$$

where U is the flux pinning energy or activation energy for flux creep depending on the temperature and magnetic field, ρ_0 is the pre-exponential factor, and k_B is

Boltzmann constant. The U value can be directly deduced from the slope of the plot of log (ρ/ρ_0) versus 1/T as exhibited in Fig. 7, where the value of ρ_0 at the temperature of 110 K was used.

The flux pinning energy or activation energy U can be calculated from the linear data in the tail part of the plots in Fig. 7, for all samples. As can be seen from the figure the activation energy, U, decreases with the increasing of the amount Yb and the applied magnetic field. It can be at the grain boundaries which reduce the intergranular coupling and increase the weak links, the vortices creep easily whereas the pinning energy or activation energy decreases. These results are in agreement with the previously reported results [19,24,67].

It will also be very useful to mention the main differences between curves in Fig. 8 observed for 0.5 Tesla applied fields. Since 0.5 Tesla, the applied magnetic field has penetrated intergranular media; a possible interpretation for the differences [19,71,72] between curves can be fit to the existence of different superconducting levels within the samples at the intergranular region. It is clear that when the magnetic field is gradually increased from 0 to 5 T, the rate of decline in pinning energy, U, decreases. Thus, it would be reasonable to assure that in the sample A, the fraction of grains interconnected by strong-links (clusters) is very small as compared with the sample D.

4 Conclusions

In the present study, $Bi_2Sr_2CaCu_{2-x}Yb_xO_y$ (x = 0.0, 0.05, 0.1, and 0.25) samples were successfully prepared by a polymer matrix route technique and then textured a (LFZ) method. The electrical resistivity broadening behavior in the magnetic field has been studied in the thermally activated flux creep model. According to this model, the flux pinning energy, U, decreases with Yb content because of reduced energy barriers. It is possible to say that the reduction of the energy barriers may arise from the increasing of the weak links. With the increase of the weak links, the vortices creep easily and the pinning energy or activation energy decreases since non-strong pinning centers are developed in the system by substitution of Yb.

Acknowledgments

This work is supported by Research Fund of Cukurova University, Adana, Turkey, under grant contracts no: FEF2011D21. A. Sotelo and M. A. Madre wish to thank the Gobierno de Aragon (Research Group T12), for financial support. M. A. Madre also acknowledges the MINECO-FEDER (Project MAT2011-22719) for funding. The authors thank to Prof. Dr. Cabir Terzioglu from Abant Izzet Baysal University for his help during the magnetoresistance measurements.

References

1. B. Chattop adhyay, B. Bandyopadhyay, A. Poddar, P. Mandal, A.N. Das, B. Ghosh, Phys. C. 331, 38 (2000)

2. G. Ilonca, V. Toma, T.R. Yang, A.V. Pop, P. Balint, M. Bodea, E. Macocian, Phys. C. 369, 460 (2007)

3. X.L. Wang, J. Horvat, G.D. Gu, K.K. Uprety, H.K. Liu, S.X. Dou, Phys. C. 337, 221 (2000)

4. T. Yamamoto, I. Kakeya, K. Kadowaki, Phys. C. 460–462, 799 (2007)

5. A. Coskun, A. Ekicibil, B. Ozcelik, Chin. Phys. Lett. 19(12), 1863 (2002)

6. D. Yazıcı, B. Ozc¸elik, M.E. Yakıncı, J. Low Temp, Phys. 163, 370 (2011)

7. H. Sozeri, N. Ghazanfari, H. Ozkan, A. Kılıc¸, Supercond. Sci. Technol. 20, 522 (2007)

8. L. Jiang, Y. Sun, X. Wan, K. Wang, G. Xu, X. Chen, K. Ruan, J. Du, Phys. C. 300, 61 (1998)

9. M. Zargar Shoushtari, S.E. Mousavi Ghahfarokhi, J. Supercond. Nov. Magn. 24, 1505 (2011)

10. A.I. Abou-Aly, M.M.H. Abdel Gawad, R. Awad, I. G-Eldeen, J. Supercond. Nov. Magn. 24, 2077 (2011)

11. S. Sakiroglu, K. Kocabas¸, J. Supercond. Nov. Magn. 24, 1321 (2011)

12. S.M. Khalil, J. Phys. Chem. Solids 62, 457 (2001)

13. C. Terzioglu, H. Aydin, O. Ozturk, E. Bekiroglu, I. Belenli, Phys. B 403, 3354 (2008)

14. M.A. Aksan, M.E. Yakıncı, Y. Balcı, J. Supercond. 15, 553 (2002)

15. M.A. Aksan, M.E. Yakıncı, Y. Balcı, Supercond. Sci. Technol. 13, 955 (2000)

16. M.E. Yakıncı, Condens. Matter. J Phys. 9, 1105 (1997)

17. A. Ekicibil, A. Coskun, B. Ozcelik, K. Kiymac, J. Low Temp, Phys. 140, 105 (2005)

18. H. Gundogmus¸, B. Ozcelik, B. Ozkurt, A. Sotelo, M.A. Madre, J. Supercond. Nov. Magn. 26, 111 (2013)

19. P.W. Anderson, Phys. Rev. Lett. 9, 309 (1962)

20. M. Erdem, O. Ozturk, E. Yucel, S.P. Altintas, A. Varilci, C. Terzioglu, I. Belenli, Phys. B 406, 705–709 (2011)
21. M. Tinkham, Phys. Rev. Lett. 61, 1658 (1988)
22. T.T. Palstra, B. Batlogg, R.B. Van Dover, L.F. Scheemeyer, J.V. Waszczak, Appl. Phys. Lett. 54, 763 (1989)
23. D.H. Kim, K.F. Gray, R.T. Kampwirth, D.M. Mckay, Phys. Rev. B. 42, 6249 (1990)
24. B. Ozkurt, B. Ozcelik, J. Low Temp, Phys. 156, 22 (2009)
25. D. Yazici, M. Erdem, B. Ozcelik, J. Supercond. Nov. Magn. 25, 1811 (2012)
26. D. Sharma, R. Kumar, V.P.S. Awana, Solid State Commun. 152, 941–946 (2012)
27. M.R. Mohammadizadeh, M. Akvahan, Phys. C. 390, 134 (2003)
28. T.T.M. Palstra, B. Batlogg, L.F. Schneemeyer, J.V. Waszczak, Phys. Rev. Lett. 61, 1662–1665 (1988)
29. Malozemoff AP, Worthington TK, Zeldov E,Yeh NC, McElfresh MW (1989) In: Fukuyama H, Maekawa S, Malozemoff AP (ed). Strong Correlation and Superconductivity, Springer Series in Sol.State Sci, vol. 89, Springer, Berlin
30. R. Griessen, Phys. Rev. Lett. 64, 1674 (1990)
31. R.C. Ma et al., Phys. C. 405, 34 (2004)
32. A. Sotelo, Sh Rasekh, M.A. Madre, J.C. Diez, J. Supercond. Nov. Magn. 24, 19–25 (2011)
33. G.F. de la Fuente, A. Sotelo, Y. Huang, M.T. Ruiz, A. Badia, L.A. Angurel, F. Lera, R. Navarro, C. Rillo, R. Ibanez, D. Beltran, F. Sapin˜a, A. Beltran, Phys. C 509, 185 (1991)
34. Ozcelik B, Ozkurt B, Yakıncı ME, Sotelo A, Madre MA J. Supercond. Nov. Magn. doi:10.1007/s10948-012-1874-9
35. A. Sotelo, H. Szillat, P. Majewski, F. Aldinger, Supercond. Sci. Technol. 10, 717–720 (1997)
36. S. Marinel, D. Bourgault, O. Belmont, A. Sotelo, G. Desgardin, Phys. C. 315, 205–214 (1999)
37. V. Garnier, R. Caillard, A. Sotelo, G. Desgardin, Phys. C. 319, 197–208 (1999)

38. A. Sotelo, M. Mora, M.A. Madre, J.C. Diez, L.A. Angurel, G.F. de la Fuente, J. Eur. Ceram. Soc. 25, 2947–2950 (2005)
39. M.A. Madre, H. Amaveda, M. Mora, A. Sotelo, L.A. Angurel, J.C. Diez, Bol. Soc. Esp. Ceram V. 47(3), 148–152 (2008)
40. G.F. de la Fuente, M.T. Ruiz, A. Sotelo, A. Larrea, R. Navarro, Mater. Sci. Eng. A. 173(1–2), 201–204 (1993)
41. M.F. Carrasco, F.M. Costa, R.F. Silva, F. Gimeno, A. Sotelo, M. Mora, J.C. Diez, L.A. Angurel, Phys. C. 415, 163 (2004)
42. R. Funahashi, I. Matsubara, K. Ueno, H. Ishikawa, Phys. C. 311, 107 (1999)
43. L.A. Angurel, J.C. Diez, G.F. de la Fuente, F. Gimeno, F. Lera, C. Lopez-Gascon, E. Martinez, M. Mora, R. Navarro, A. Sotelo, N. Andres, S. Recuero, M.P. Arroyo, Phys. Status Solidi A. 203, 2931–2937 (2006)
44. Kaya C, Ozcelik B,Ozkurt B, Sotelo A, Madre MA (2012) J. Mater Sci: Mater. Electron. doi:10.1007/s10854-012-0979-z
45. S. Vinu, P.M. Sarun, A. Biju, R. Shabna, P. Guruswamy, U. Syamaprasad, Supercond. Sci. Technol. 21, 045001 (2008)
46. S. Vinu, P.M. Sarun, R. Shabna, A. Biju, U. Syamaprasad, Mater. Lett. 62, 4421 (2008)
47. R. Shabna, P.M. Sarun, S. Vinu, A. Biju, U. Syamaprasad, Supercond. Sci. Technol. 22, 045016 (2009)
48. A. Ekicibil, S.K. Cetin, A.O. Ayas¸, A. Coskun, T. Fırat, K. Kıymac¸, Solid State Sci. 13, 1954 (2011)
49. B.D. Cullity, Element of X-ray differaction (Addition-Wesley, Reading, 1978)
50. M.R. Presland, J.L. Tallon, R.G. Buckley, R.S. Liu, N.E. Floer, Phys. C 176, 95 (1991)
51. D. Yazici, B. Ozcelik, J. Supercond. Nov. Magn. 25, 293 (2012)
52. G. Yildirim, S. Bal, A. Varilci, J. Supercond. Nov. Magn. 25, 1665 (2012)
53. R. Awad, A.I. Abou-Aly, M.M.H. Abdel Gawad, I. G-Eldeen, J. Supercond. Nov. Magn. 25, 739 (2012)
54. A.I. Abou-Aly, M.F. Mostafa, I.H. Ibrahim, R. Awad, M.A. Al-Hajji, Supercond. Sci. Technol. 15, 9384 (2002)

55. A.V. Pop, D. Ciurchea, G. Ilonca, A. Harabor, R. Deltour, Phys. C. 282–287, 2365 (1997)
56. A. Ianculescu, M. Gartner, B. Despax, V. Bley, Th Lebey, R. Gavrila, M. Modreanu, Appl. Surf. Sci. 253, 344 (2006)
57. M. Tinkham, Introduction to Superconductivitiy, 2nd edn. (McGraw-Hill, New York, 1996)
58. Y. Liu, X.G. Li, J. Appl. Phys. 99, 053903 (2006)
59. A. Jukna, I. Barboy, G. Jung, S.S. Banerjee, Y. Myasoedov, V. Plausinaitiene, A. Abrutis, X. Li, D. Wang, R. Sobolewski, Appl. Phys. Lett. 87, 192504 (2005)
60. B. Ozkurt, A. Ekicibil, M.A. Aksan, B. Ozcelik, M.E. Yakıncı, K. Kıymac¸, J. Low, Temp. Phys. 149, 105 (2007)
61. Sotelo A, Madre MA, Rasekh Sh, Constantinescu G, Torres MA, Diez JC J. Supercond. Nov. Magn. doi:10.1007/s10948-012-1922-5
62. M. Mudgel, L.S. Sharath Chandra, V. Ganesan, G.L. Bhalla, H. Kishan et al., J. Appl. Phys. 106, 033904 (2009)
63. N.R. Werthamer, E. Helfand, P.C. Hohenberg, Phys. Rev. 147, 295 (1966)
64. Yang HC, Wang LM (1999) Phys Rev B 59, N 13
65. M. Xianglei et al., Condens. Matter. J. Phys. 3, 3511 (1991)
66. J.G. Chigvinadze, A.A. Iashvili, T.V. Machaidze, Phys. Lett. A 300, 524 (2002)
67. D. Yazici, M. Erdem, B. Ozcelik, J. Supercond. Nov. Magn. 25, 725 (2012)
68. P.W. Anderson, Phys. Rev. Lett. 9, 309 (1962)
69. P.W. Anderson, Y.B. Kim, Rev. Mod. Phys. 36, 39 (1964)
70. T.P. Sheahen, Introduction to High-Temperature Superconductivity (Kluwer Academic, Dordrecht, 2002)
71. E. Govea-Alcaide, I. Garcia-Fornaris, P. Mune, R.F. Jardim, Eur. Phys. J. B 58, 373 (2007)
72. P. Mune, E. Govea-Alcaide, R.F. Jardim, Phys. C. 384, 491 (2003)

Table 1. Unit cell parameters, particle size and hole-carrier concentration for each of the samples

Sample	a = b (Å)	c (Å)	L_{hkl} (Å)	*p* (Hole number)
A	3.834	30.950	371.1391	0.144
B	3.832	30.939	364.5567	0.138
C	3.832	30.900	332.2064	0.135
D	3.832	30.850	319.1931	0.135

Table 2. T_c^{onset} and T_c^{offset} values of the samples at various applied magnetic field

Samples	0 Tesla	0.5 Tesla	1 Tesla	5 Tesla
A	$T_c^{\text{onset}} = 100$ K	$T_c^{\text{onset}} = 99$ K	$T_c^{\text{onset}} = 98$ K	$T_c^{\text{onset}} = 97$ K
	$T_c^{\text{offset}} = 95$ K	$T_c^{\text{offset}} = 89.5$ K	$T_c^{\text{offset}} = 87.9$ K	$T_c^{\text{offset}} = 78$ K
B	$T_c^{\text{onset}} = 98.6$ K	$T_c^{\text{onset}} = 96.7$ K	$T_c^{\text{onset}} = 93$ K	$T_c^{\text{onset}} = 92$ K
	$T_c^{\text{offset}} = 93.2$ K	$T_c^{\text{offset}} = 79$ K	$T_c^{\text{offset}} = 74.5$ K	$T_c^{\text{offset}} = 63$ K
C	$T_c^{\text{onset}} = 97.7$ K	$T_c^{\text{onset}} = 90$ K	$T_c^{\text{onset}} = 88$ K	$T_c^{\text{onset}} = 86$ K
	$T_c^{\text{offset}} = 92.1$ K	$T_c^{\text{offset}} = 67$ K	$T_c^{\text{offset}} = 65$ K	$T_c^{\text{offset}} = 56$ K
D	$T_c^{\text{onset}} = 96$ K	$T_c^{\text{onset}} = 89$ K	$T_c^{\text{onset}} = 85$ K	$T_c^{\text{onset}} = 82$ K
	$T_c^{\text{offset}} = 90$ K	$T_c^{\text{offset}} = 64$ K	$T_c^{\text{offset}} = 62$ K	$T_c^{\text{offset}} = 48$ K

Figure captions

Figure 1. X-ray diffraction patterns of the $Bi_2Sr_2CaCu_{2-x}Yb_xO_y$ superconducting samples. (+) Bi-2212 phase, and (*) $(Sr,Ca)CuO_2$ secondary phases

Figure 2. Magnetization against temperature for samples a, b, c and d at an applied field of 50 Oe

Figure 3. Temperature dependence of resistivity for various applied magnetic field for sample a, b, c and d

Figure 4. The irreversibility lines of the samples a, b, c and d for T_c^{onset} and T_c^{offset}

Figure 5. Upper critical magnetic field $H_{C2}(T)$ versus T_c for the samples

Figure 6. H_{C2} and ξ values versus Yb content

Figure 7. The Arrhenius plot of the resistivity of samples a, b, c and d

Figure 8. The flux pinning energy U versus applied magnetic for the samples

Figure 1

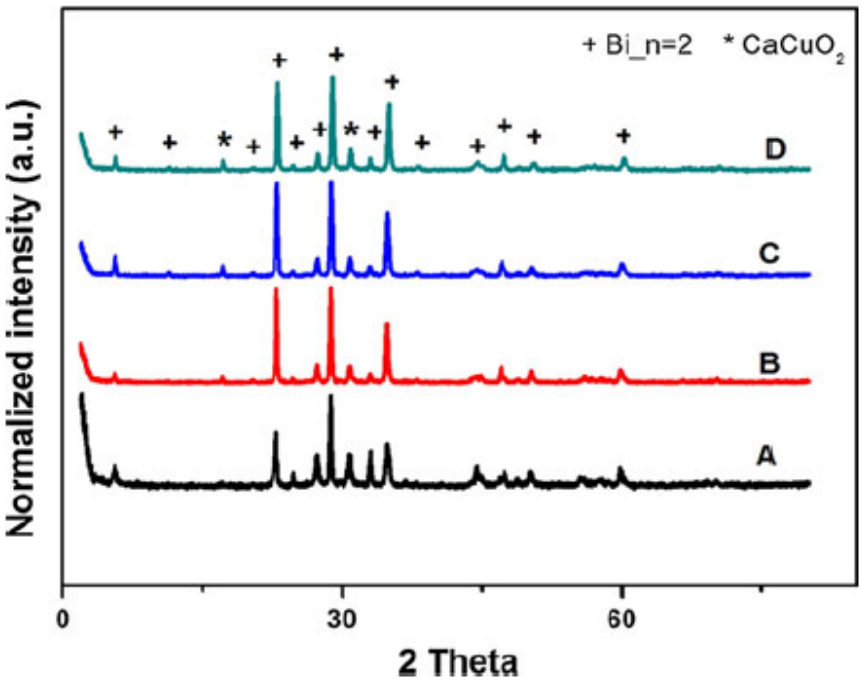

Figure 2

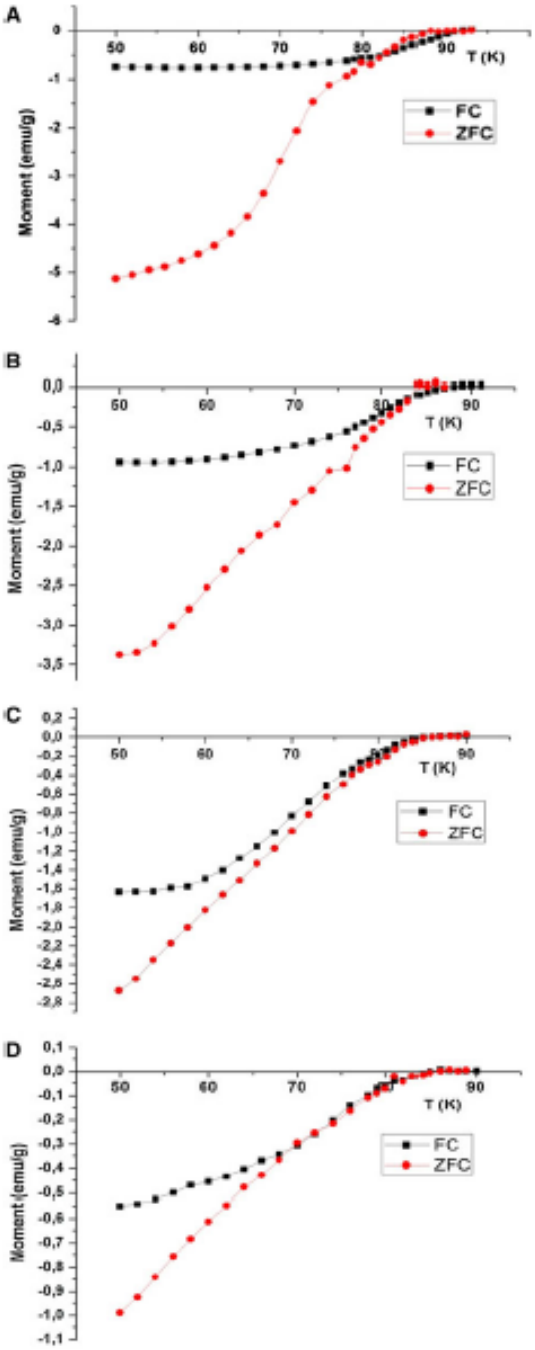
A
Moment (emu/g)
T (K)
FC
ZFC
B
Moment (emu/g)
T (K)
FC
ZFC
C
Moment (emu/g)
T (K)
FC
ZFC
D
Moment (emu/g)
T (K)
FC
ZFC

Figure 3

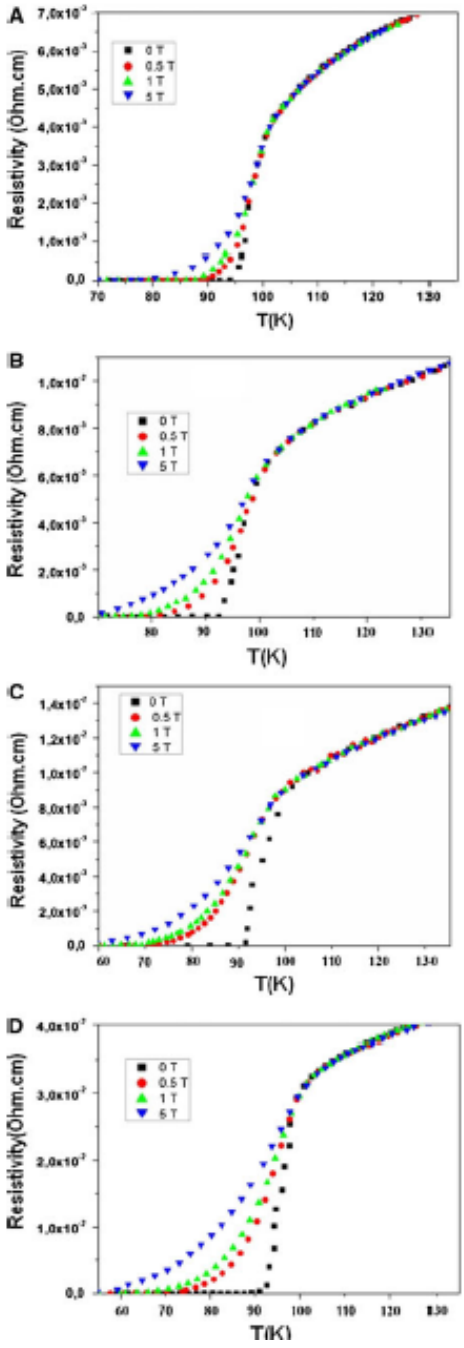

Figure 4

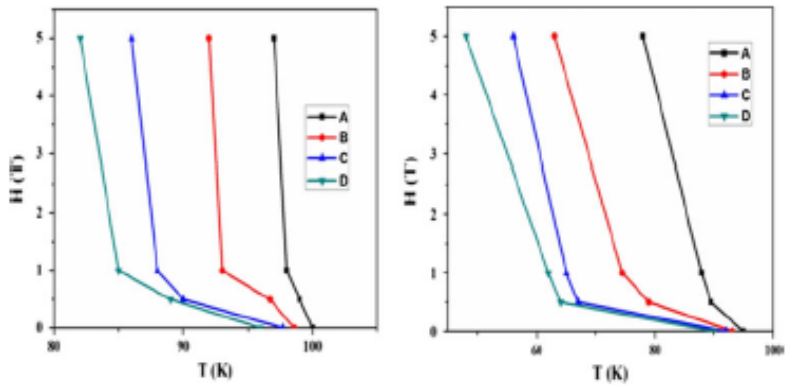

Figure 5

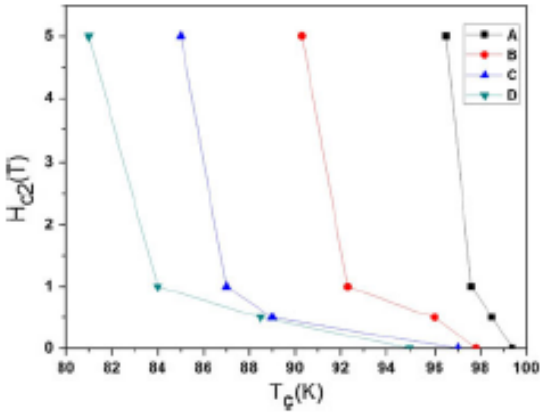

Figure 6

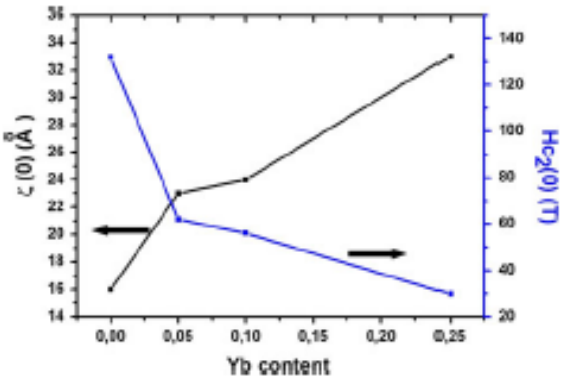
ξ (0) (Å)
Hc2(0) (T)
Yb content
0,00
0,05
0,10
0,15
0,20
0,25
14
16
18
20
22
24
26
28
30
32
34
36
20
40
60
80
100
120
140

Figure 7

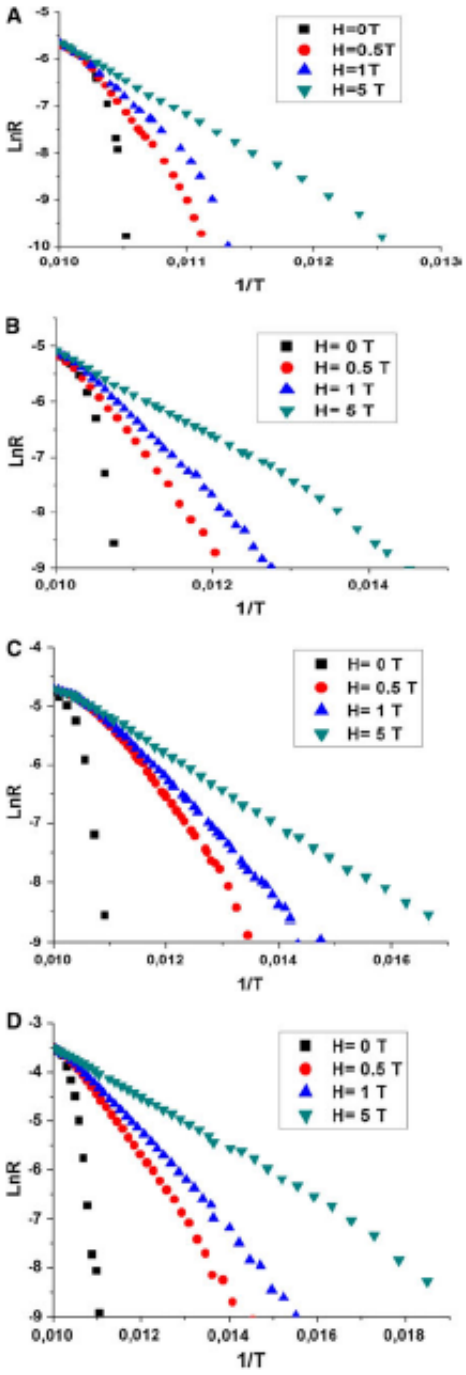
A
H=0T
H=0.5T
H=1T
H=5 T
LnR
1/T
B
H= 0 T
H= 0.5 T
H= 1 T
H= 5 T
LnR
1/T
C
H= 0 T
H= 0.5 T
H= 1 T
H= 5 T
LnR
1/T
D
H= 0 T
H= 0.5 T
H= 1 T
H= 5 T
LnR
1/T

Figure 8